

RADIO VARIABILITY IN SEYFERT NUCLEI

C.G. MUNDELL¹, P. FERRUIT², N. NAGAR³ AND A.S. WILSON⁴

¹ Astrophysics Research Institute, Liverpool John Moores University, Twelve Quays House, Egerton Wharf, Birkenhead, CH41 1LD, U.K: cgm@astro.livjm.ac.uk

² Observatoire de Lyon, 9 Avenue Charles André, Saint-Genis Laval Cedex, F69561, France

³ Astronomy Group, Departamento de Física, Universidad de Concepción, Casilla 160-C, Concepción, Chile and

⁴ University of Maryland, College Park, MD20742, U.S.A.

Received 2008 November 27; accepted 2009 June 22; published 2009

ABSTRACT

Comparison of 8.4-GHz radio images of a sample of eleven, early-type Seyfert galaxies with previous observations reveals possible variation in the nuclear radio flux density in five of them over a seven year period. Four Seyferts (NGC 2110, NGC 3081, MCG -6-30-15 and NGC 5273) show a decline in their 8.4-GHz nuclear flux density between 1992 and 1999, while one (NGC 4117) shows an increase; the flux densities of the remaining six Seyferts (Mrk 607, NGC 1386, Mrk 620, NGC 3516, NGC 4968 and NGC 7465) have remained constant over this period. New images of MCG -5-23-16 are also presented. We find no correlation between radio variability and nuclear radio luminosity or Seyfert nuclear type, although the sample is small and dominated by type 2 Seyferts. Instead, a possible correlation between the presence of nuclear radio variability and the absence of hundred parsec-scale radio emission is seen, with four out of five marginally-resolved or unresolved nuclei showing a change in nuclear flux density, while five out of six extended sources show no nuclear variability despite having unresolved nuclear sources. NGC 2110 is the only source in our sample with significant extended radio structure and *strong* nuclear variability ($\sim 38\%$ decline in nuclear flux density over seven years). The observed nuclear flux variability indicates significant changes are likely to have occurred in the structure of the nucleus on scales smaller than the VLA beam size (i.e. within the central 15 pc), between the two epochs, possibly due to the appearance and fading of new components or shocks in the jet, consistent with previous detection of sub-parsec scale nuclear structure in this Seyfert. Our results suggest that all Seyferts may exhibit variation in their nuclear radio flux density at 8.4 GHz, but that variability is more easily recognised in compact sources in which emission from the variable nucleus is not diluted by unresolved, constant flux density radio-jet emission within the central $\lesssim 50$ pc. If flares in radio light curves correspond to ejection of new relativistic components or emergence of shocks in the underlying flow, improved monitoring and high resolution imaging using VLBI techniques are required to confirm that radio jets are intrinsically non-relativistic during quiescence but that Seyferts, as black-hole driven AGN, have the capacity to accelerate relativistic jets during radio flares. Finally, we conclude that our results taken together with the increased detection rate of flat spectrum radio nuclei in Seyferts imaged at VLBI resolutions and the detection of variable water megamaser emission support the paradigm of intermittent periods of quiescence and nuclear outburst across the Seyfert population.

Subject headings: galaxies: active – galaxies: jets – galaxies: Seyfert – radio continuum: galaxies

1. INTRODUCTION

Variability of nuclear flux density at all wavelengths across the electromagnetic spectrum has long been recognized as a defining characteristic of active galactic nuclei (AGN) (e.g. Smith & Hoeffleit 1963). The short variability timescales measured at X-ray, optical and UV wavelengths, ranging from days to years depending on observing wavelength and intrinsic AGN luminosity, support the standard AGN paradigm of nuclear emission originating from compact regions powered by accretion of matter by a central supermassive black hole, rather than standard stellar processes (e.g. Ulrich et al. 1997; Sambruna et al. 1999; Gliozzi et al. 2003).

Variability at radio wavelengths is most marked in powerful radio-loud AGN. The largest and most rapid variations observed in nuclear non-thermal continuum emission is seen in BL Lacs and core-dominated quasars (e.g. Lister 2001, and references therein). These variations are explained primarily by Doppler boost-

ing of the nuclear emission by highly-relativistic jets viewed at small angles to the line of sight and are consistent with radio-loud Unification Schemes (e.g. Orr & Browne 1982). Flares in the radio light curves might correspond to ejection of new relativistic components or emergence of shocks in the underlying flow (e.g. Brunthaler et al. 2000; Valtaoja et al. 2002).

Seyfert nuclei, classified as radio quiet though not radio silent, have been known for some time to show variability in their continuum and line emission at X-ray, optical and UV wavelengths (e.g. Turner et al. 1999; Wandel et al. 1999; Nandra et al. 2000; Peterson et al. 2000; Shemmer et al. 2001; McHardy et al. 2005; Wheatley et al. 2008), providing constraints on the variation of nuclear absorbing column, photon reprocessing, structure and dynamics of the broad line region and ultimately the mass of the central object. However, little is known about radio variability in Seyfert nuclei as only a small number of ‘interesting’ Seyferts have

TABLE 1
VLA OBSERVING PARAMETERS

Galaxy	Phase	Field Center	Cycle time	Time on Source
	Calibrator	RA , Dec (B1950)	(minutes)	(minutes)
Mrk 607	0336–019	03 22 17.77, –03 13 04.8	14.4 + 1.4	140
NGC 1386	0332–403	03 34 51.80, –36 09 47.1	10.5 + 1.5	160
NGC 2110	0539–057	05 49 46.38, –07 28 02.0	9.5 + 1.5	130
Mrk 620	0646+600	06 45 37.63, +60 54 12.8	14.4 + 1.4	140
MCG–5–23–16	0919–260	09 45 28.32, –30 42 59.0	14.6 + 1.6	140
NGC 3081	1032–199	09 57 09.94, –22 35 10.6	14.5 + 1.5	140
NGC 3516	1044+719	11 03 22.81, +72 50 20.5	10.4 + 1.4	140
NGC 4117	1144+402	12 05 14.13, +43 24 16.1	14.5 + 1.5	140
NGC 4968	1256–220	13 04 23.92, –23 24 35.1	14.5 + 1.5	140
MCG–6–30–15	1313–333	13 33 01.84, –34 02 25.7	9.4 + 1.4	132
NGC 5273	1328+307	13 39 55.15, +35 54 21.7	14.5 + 1.5	140
NGC 7465	2251+158	22 59 32.03, +15 41 44.4	14.5 + 1.5	140

been systematically monitored at radio frequencies (e.g. Neff & de Bruyn 1983; Wrobel 2000), with some studies motivated by serendipitous discovery of radio flares (Falcke et al. 1998; Falcke et al. 2000).

Here we present the results of a two-epoch study of 8.4-GHz nuclear radio emission in a small, but complete sample of 11 nearby optically-selected Seyferts in which the nuclear radio emission is imaged at angular resolutions of $\sim 0''.2$ (< 50 pc); the original goal of the study was to obtain high quality radio images to investigate the impact of Seyfert radio jets on the interstellar medium by comparing extended radio structures with extended ionised gas distributions and excitations in the narrow line region as inferred from images with the *Hubble Space Telescope* (*HST*) by Ferruit, Wilson & Mulchaey (2000). We provide such a comparison here, including new radio images of MCG –5-23-16. However, by more reliably separating nuclear and extended radio components and comparing with previous nuclear flux density measurements we serendipitously discovered a fraction of Seyfert nuclei with variable nuclear radio flux densities. It is primarily this result that we present here.

VLA and MERLIN observations and data reduction are described in Section 2 with the results of the VLA radio imaging, individual source properties and comparison with HST emission-line maps presented in Section 3. In Section 4, we discuss the nuclear radio variability and its possible relationship to radio jet properties and the small number of previously-studied radio flares in Seyfert nuclei. Conclusions are presented in Section 5. A Hubble constant of $H_0 = 75 \text{ km s}^{-1} \text{ Mpc}^{-1}$ is used throughout.

2. OBSERVATIONS AND DATA REDUCTION

2.1. Sample Selection

We have selected a set of 12 Seyfert galaxies, which forms a sub-sample of Mulchaey’s sample of early-type Seyfert galaxies (Mulchaey et al. 1996) and comprises all 12 Seyfert galaxies in early type hosts with $m_V < 14.5$, $cz < 3000 \text{ km s}^{-1}$ and declination suitable for VLA observations. The optical continuum and ionized gas properties have been studied with the *HST* (Ferruit et al. 2000); our sample is the same as that of Ferruit et al. (2000), except that two galaxies too far south to be reached by the VLA are omitted. All of our objects, except MCG –5-23-16, were observed with the VLA in 1993, at 1.4 GHz and 8.4 GHz, as part of

the larger VLA snapshot study of Nagar et al. (1999 - hereafter N99).

2.2. VLA Observations

The observations were conducted using the VLA in A configuration at 8.4 GHz on 1999 August 20 and 21 under project code AF360 (P.I.: Ferruit). Each Seyfert was observed twice, in two ~ 1 -hr segments separated in time to provide improved hour angle and (u, v) coverage. Within each segment, the standard phase referencing technique of cycling between the short exposures on the target and a nearby, bright compact radio source (phase calibrator) was used in order to correct for phase and gain variations due to instrumental and ionospheric variations. Observing parameters are given in Table 1 including the calibrator/target cycle time. All Seyferts, except NGC 3516, were observed in standard continuum mode using two intermediate-frequency channels (IFs) resulting in a total bandwidth of 100 MHz; dual circular polarizations (right and left) were recorded for all sources, and only the parallel hands (i.e., RR and LL) were correlated. In order to allow for better removal of contaminating emission from a strong confusing source 4'.3 away (see Miyaji et al. 1992), NGC 3516 was observed in spectral line mode, using 7 channels and 2 IFs resulting in a total bandwidth of 37.5 MHz after removal of end channels. Although NGC 3516 was observed for 140 minutes, data problems rendered 56 minutes of data unusable leaving 84 minutes of data available for imaging. Observations of 0134+329 (3C48) and 1328+307 (3C286) were used to determine the flux density scale using the VLA values as determined in 1995.2.

Standard data editing, calibration and analysis were performed (Greisen & Murphy 1998)¹ using the NRAO² Astronomical Image Processing System (AIPS; van Moorsel et al. 1996). Data for each IF and polarization were edited and calibrated separately before being combined and imaged. Clean components from the resultant images were then used to perform standard iterative self-calibration on the stronger sources ($S_{8.4 \text{ GHz}} \gtrsim 2 \text{ mJy}$) – NGC 1386, NGC 2110, Mrk 620, MCG –5–23–16, and NGC 4968.

¹ <http://www.cv.nrao.edu/aips/cook.html>

² The National Radio Astronomy Observatory is a facility of the National Science Foundation operated under cooperative agreement by Associated Universities, Inc.

A similar but more extensive method was used for the weaker sources – Mrk 607, NGC 3081, NGC 4117, MCG –6-30-15 and NGC 5273. Although it was possible to image the weaker sources by applying directly the interpolated phase and gain corrections derived from the phase calibrator in the standard way, it was important to examine the data for possible atmospheric decorrelation effects that could result in an apparent reduction in flux density. A number of these weaker sources were observed during the daytime in Summer when rapid phase changes at 8.4 GHz due to variations in the troposphere might occur. We therefore inspected the raw phases observed for each phase calibrator and calculated the rate of change of phase across each 1-minute scan and within a 10-s integration time. Most scans showed small phase changes $\lesssim 10\text{--}20^\circ$ per 10 s integration, resulting in amplitude reduction due to decorrelation of less than 6%. A maximum phase rate of $\sim 4^\circ \text{ s}^{-1}$ was observed on some of the longest baselines for $< 30\%$ of the time; the reduction in amplitude from decorrelation at this phase rate would be $\sim 22\%$ so data corresponding to these timeranges were excised. Assuming phase changes monotonically across a 1-minute scan (i.e. that extreme 2π phase wraps do not occur between integrations), the resultant maximum phase rates per 10-s integration for the remaining data are negligible. Atmospheric decorrelation within an integration time is therefore ruled out.

As each Seyfert was observed in two 1-hr segments, we used the observed phase rates for the associated phase calibrator to quantify the data quality for each 1-hr data segment separately. In general, each phase calibrator has very good phase stability for at least 1 hr where ‘good’ is defined as negligible phase rates within each 1-minute calibrator scan and only small, smoothly varying, phase rates between scans on most baselines. With this quality definition in mind, each hour segment was imaged separately and the final flux densities measured. As expected, the images resulting from the time range with poorer phase stability show a reduced central flux density of up to $\sim 30\%$ compared with the ‘good’ timerange, with the remaining flux density spread throughout the map. Therefore, only clean components from the ‘good’ image were used to perform phase-only self-calibration on the whole 2-hr dataset. Phases were re-examined and each 1-hr segment re-imaged separately. In all cases the self-calibration worked well for the ‘good’ hour and in the case of MCG –6-30-15 it also worked well for the ‘poor’ hour, as confirmed by the flux density in each resultant image being the same. A final image combining the full two hours was then made. In the case of NGC 3081, Mrk 607, NGC 4117 and NGC 5273, the self-calibration of the ‘poor’ hour was insufficiently good to warrant inclusion of these data in the final image and only the ‘good’ hour was used. This resulted in a higher rms noise in the final images due to the reduced exposure time, but gives a more reliable total flux density estimate, free from significant phase decorrelation effects.

As described above, NGC 3516 was observed in spectral line mode; therefore, in addition to editing and calibrating each IF and polarization separately, each narrow spectral line channel was also calibrated, edited, and imaged separately before being averaged together to form the final image ready for deconvolution. This method minimizes chromatic aberration, or bandwidth smearing,

of the confusing source and ensures correct removal of its sidelobe contribution at the phase center of the image close to NGC 3516. A Gaussian fit to the confusing source confirmed that it was unresolved and not radially smeared, therefore free from chromatic aberration. Iterative self-calibration, using the same imaging and calibration method preserving the narrow spectral channels until the last stage of imaging, was then performed on the spectral line dataset, using clean components from the final combined image.

The final calibrated (u, v) data for all sources were Fourier transformed with both natural and uniform weighting and deconvolved; the highest angular resolution images were made using uniform weighting with Briggs’ robustness parameter set to -4 (equivalent to uniform weighting) while lower resolution images, more sensitive to extended emission, were made with both natural weighting and uniform weighting with robust parameter 0. Final images (Figures 1-4) were restored with circular beams, with sizes corresponding to the mean value of the full width at half maximum of minor and major axes of the fitted beam. The data were also tapered (reducing the contribution from data points corresponding to longer baselines) to search for more extended emission; a tapered image of NGC 3516 is shown in Figure 7. Comparison of parameters derived from Gaussian fits to images restored with a fitted elliptical beam and the mean circular beam showed no difference, indicating that for most sources a circular beam is a reasonable choice. The source properties for NGC 3516 (Table 3) were derived from an image (not shown) restored with the fitted elliptical beam which has its major axis in P.A. 90° and thus maximum resolution in the north-south direction, allowing the northern component to be fully separated from the nuclear component. The integrated flux densities (Table 2) were measured from the naturally weighted images, which are most sensitive to extended structure, and individual component properties (Table 3) from uniformly weighted images, which provide maximum angular resolution. The uncertainty in the flux scale is taken to be 5% and is included in the total uncertainties in flux densities quoted in Tables 2 and 3. These errors were derived by adding, in quadrature, the conservative 5% flux scale error, the rms noise in the final image and the error in the Gaussian fitting. Contour levels, as multiples of $3\text{--}\sigma$ rms noise, and restoring beam sizes used in Figures 1 - 4 are listed in Table 4.

The original data presented in N99 were reprocessed using the methods described above to provide error estimates, not originally quoted in N99, test for any decorrelations and to enable consistent flux comparisons across the two epochs. The N99 data were obtained during winter months when decorrelation is less severe, consistent with our tests; we verified this in particular for NGC 4117, thereby ruling out decorrelation as an explanation for its non-detection in 1992. All sources were observed in A configuration, except NGC 1386 and MCG –6-30-15 for which lower angular resolution data from BnA configuration were obtained. Source values for both epochs are given in Tables 2 and 3.

2.3. MERLIN Observations

We obtained and analyzed two hours of MERLIN $\lambda 21\text{-cm}$ (1.407 GHz) archival data for Mrk 620, which was

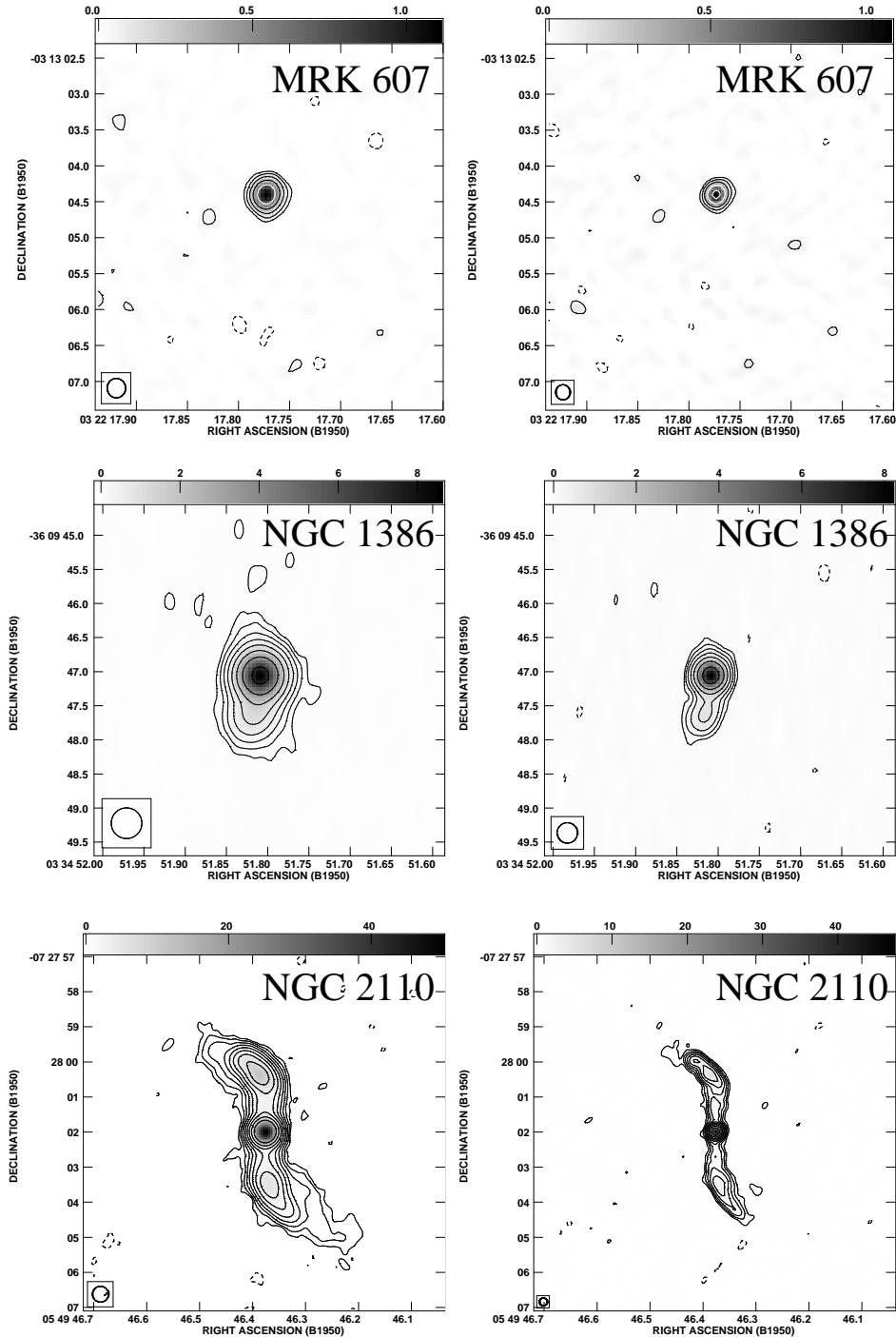


FIG. 1.— 8.4-GHz radio images of Seyferts - lower/higher resolution images are shown in the left/right column respectively. The restoring beam size is plotted in the lower left corner of each image. Table 4 gives details of restoring beam sizes and contour levels used.

observed on 1998 May 9 with seven antennas including the Lovell telescope. The data were processed using standard methods (e.g. Mundell et al. 2001), including self-calibration and re-weighting of the antennas according to their gains. The presence of weak extended emission on the shorter spacings and the small amount of data (restricted (u, v) coverage) made self-calibration and reliable imaging of weaker features difficult; nevertheless flux densities of the brighter eastern and western compo-

nents, measured from a $0''.2$ -resolution image, were used to calculate the spectral index between 1.4 GHz and 8.4 GHz at this resolution.

3. RESULTS

All 12 Seyfert nuclei in our sample are detected at 8.4 GHz with the VLA. For the eleven Seyferts with two epochs of observations, four nuclei, NGC 2110, NGC 3081, MCG -6-30-15 and NGC 5273, show a decline

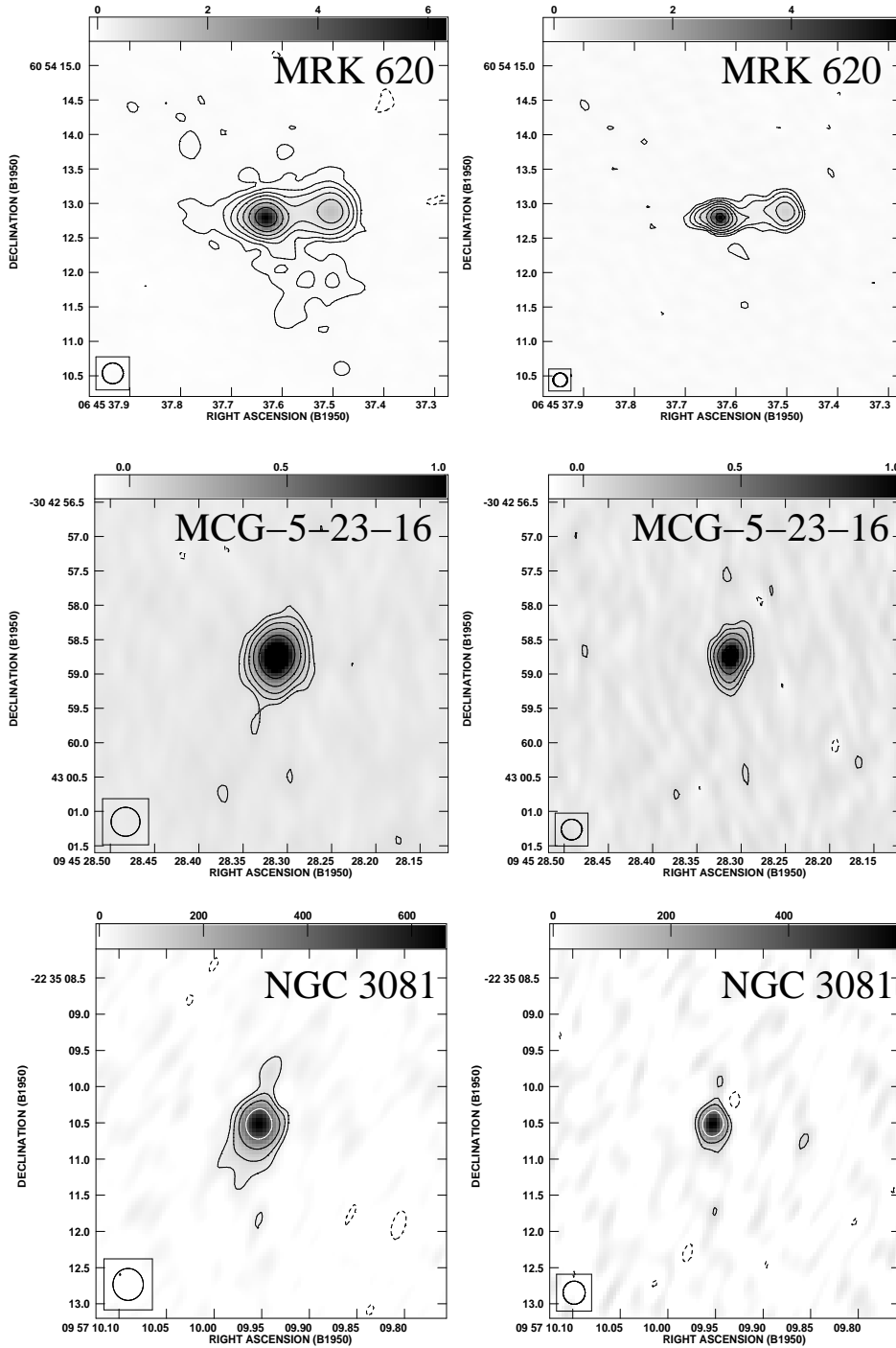


FIG. 2.— 8.4-GHz radio images of Seyferts; see Table 4 for contour levels.

in their nuclear 8.4 GHz flux density between 1992 and 1999, while NGC 4117 shows an increase; the flux densities of the remaining six Seyferts, Mrk 607, NGC 1386, Mrk 620, NGC 3516, NGC 4968 and NGC 7465, have remained constant over this period. Here we describe the radio properties of each Seyfert galaxy, comparing the present data with earlier 8.4-GHz measurements by N99; sources with spatially extended radio emission are compared with their optical line-emission images.

3.1. Notes on Individual Sources

Mrk 607 (NGC1320) - Seyfert type 2 - We confirm the presence of a small, weak extension to the south of the nucleus, visible in the naturally weighted image (Figure 1), which was previously noted by N99 but presumed to be an artefact; Gaussian fitting to the image suggests the source is marginally resolved in PA 158° with a deconvolved size of 140 mas, although this value is uncertain due to the weakness of the extended feature. The

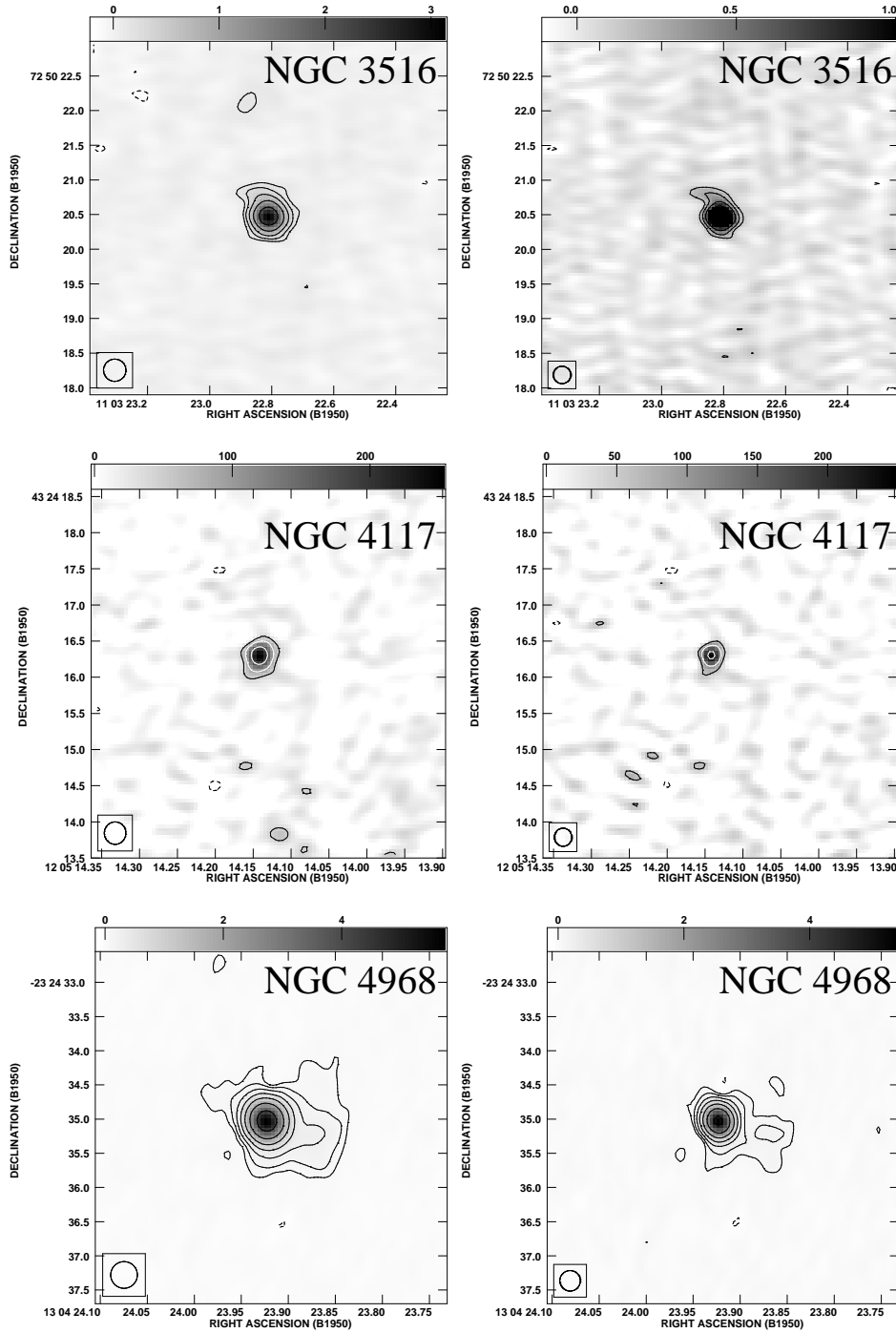


FIG. 3.— 8.4-GHz radio images of Seyferts; see Table 4 for contour levels.

slightly higher flux density of 1.3 mJy measured in the natural image compared with 1.2 mJy measured in the uniform image (Figure 1) also suggests the possible presence of weak extended emission. The total flux density of Mrk 607 measured in 1999 remains the same as that measured in 1992 at 1.3 mJy.

Emission-line images (Ferruit et al. 2000) show a ridge of ionised gas extending up to $2''$ northwest of the nucleus, along the galaxy major axis, with the $[\text{O III}]/[\text{N}$

$\text{II}]+\text{H}\alpha$ ratio peaking at the nucleus. The anti-correlation between the extended radio emission and ionised gas, the high excitation level of the nuclear optical line emission and the small linewidths of low and medium excitation lines (De Robertis & Osterbrock 1986) suggest that the line-emitting gas is photo-ionised by the nucleus and not by the passage of the radio jet.

NGC 1386 - Seyfert type 2 - A clear extension to the south of the nucleus is seen in both natural and uniform

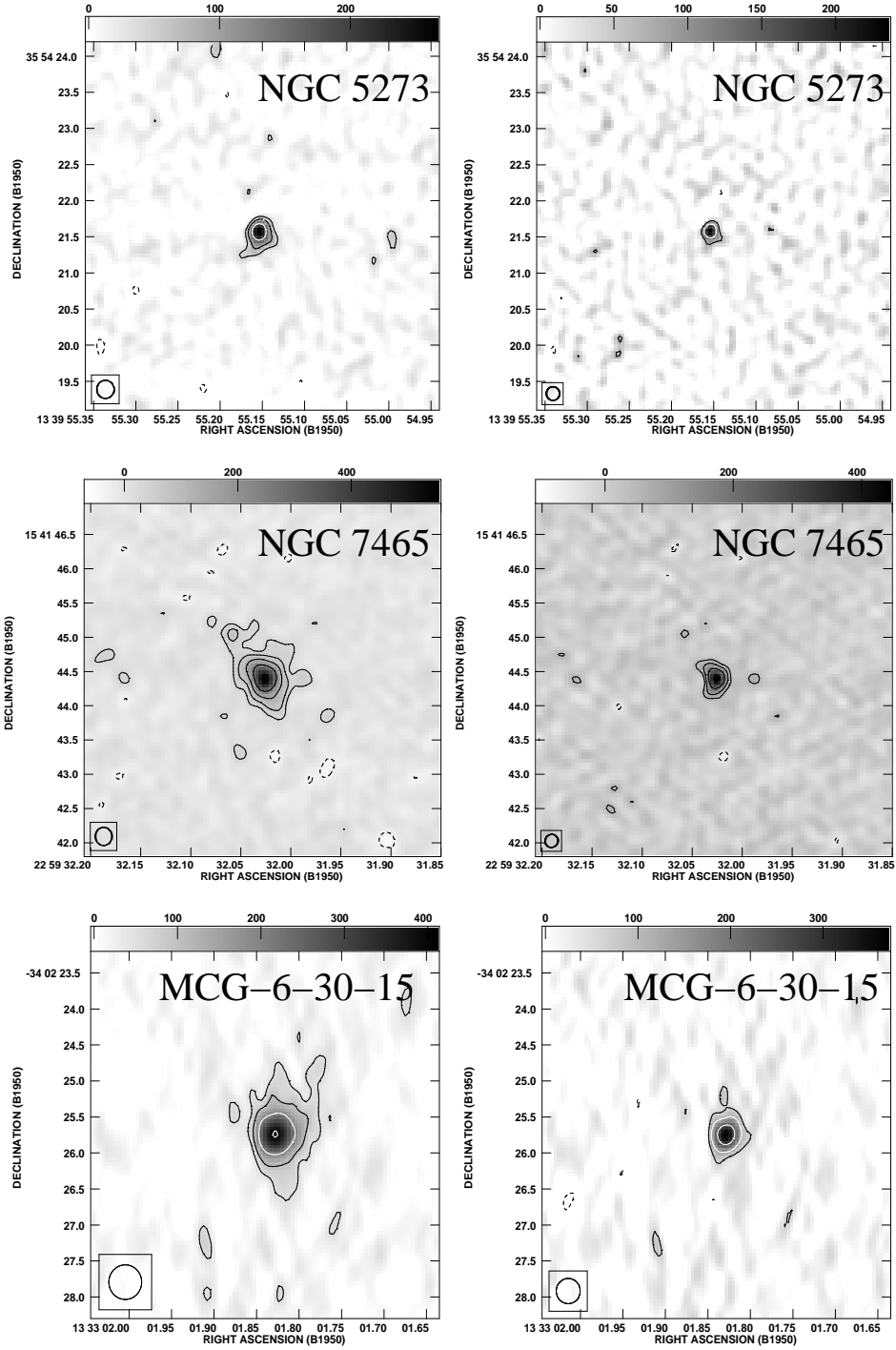


FIG. 4.— 8.4-GHz radio images of Seyferts; see Table 4 for contour levels.

radio images (Figure 1), confirming the detection by N99. The low declination of the source results in a beam elongated in the north-south direction, i.e. approximately along the source extension direction. Nevertheless, the source is sufficiently bright for an average circular restoring beam to show the extension clearly. Fitted parameters are consistent with those derived from a uniform image with elliptical beam (not shown). The unresolved nuclear flux density is 9.0 mJy and the southern component

has a flux density of 1.3 mJy with its peak lying $\sim 0''.52$ south of the nucleus in PA $\sim 175^\circ$. Extended emission is also marginally resolved to the north of the nucleus as can be seen in Figure 5, which shows the naturally-weighted residual radio image of NGC 1386 after subtraction, in the (u, v) plane, of a 7.3 mJy point source centred at the position marked “+”. It is unlikely that there has been any variation in nuclear flux density between 1992 and 1999 (see Table 3) and the higher total flux density in

TABLE 2
RESULTS OF 8.4 GHz OBSERVATIONS AND COMPARISON WITH PREVIOUS OBSERVATIONS

Galaxy	Other	R.A. (B1950)	Dec. (B1950)	S (mJy) (1999)	S (mJy) (1992)	Radio Structure	Variable nucleus?	Seyfert type
Mrk 607	NGC 1320	03 22 17.77	-03 13 04.4	1.3±0.07	1.3±0.2	(S)	No	2
NGC 1386	ESO 358-G35	03 34 51.81	-36 09 47.1	10.3±0.5	9.1±0.6	L	No	2
NGC 2110	MCG-1-15-4	05 49 46.38	-07 28 02.0	101.6 ±5.1	130.9±6.5	L	Decline	2
Mrk 620	NGC 2273	06 45 37.63	+60 54 12.8	13.5±0.7	11.4±0.6	L+D	No	2
MCG-5-23-16	ESO 434-G40	09 45 28.31	-30 42 58.8	2.1 ±0.1	-	(S)	-	2
NGC 3081	ESO 499-IG31	09 57 09.95	-22 35 10.6	0.72±0.05	1.35±0.1	(S)	Decline	2
NGC 3516	UGC 6153	11 03 22.81	+72 50 20.5	3.9±0.21	4.1±0.2	L	No	1.2
NGC 4117	UGC 7112	12 05 14.14	+43 24 16.3	0.3±0.05	<0.1	U	Increase	2
NGC 4968	MCG-4-31-30	13 04 23.92	-23 24 35.0	7.8±0.7	7.4±0.4	S+D	No	2
MCG-6-30-15	ESO 383-G35	13 33 01.83	-34 02 25.7	0.64±0.05	1.0±0.1	(S)	Decline	1.2
NGC 5273	UGC 8675	13 39 55.15	+35 54 21.6	0.38±0.06	0.64±0.08	(S)	Decline	1.5
NGC 7465	UGC 12317	22 59 32.03	+15 41 44.4	1.2±0.1	1.4±0.1	S	No	2

Notes. Galaxy names, alternative names, positions and total integrated fluxes measured in 1999 are listed (columns [1]–[5]). Listed for comparison (column [6]) are the total integrated fluxes measured in 1992 by Nagar et al. (1999) corrected by a factor of 1.006 to correct for the small difference in absolute flux scale calibration adopted by N99 and the present paper. The radio source structure (Column [7]) in the 8.4 GHz images is listed, following the classification definitions of Ulvestad & Wilson (1984a) where L = linear source, S = slightly resolved, D = diffuse and U = unresolved; sources which are less than one half the beam size after deconvolution but show a possible extension in the 3.6 cm image are tentatively considered to be slightly resolved (S). Any variability in flux density of the nuclear component between the 1992 and 1999 observations is noted in column [8], but see text for full discussion of source properties; see also Table 3 for properties of multiple-component resolved sources. MCG-5-23-16 was not observed by N99, so no flux comparison is made here, as indicated by “-” in columns (6) and (8).

TABLE 3
RESOLVED SOURCES - COMPONENT PROPERTIES.

Galaxy	R.A. (B1950)	Dec. (B1950)	S (mJy)('99)	S (mJy)('92)	Component	Variability?
NGC 1386	03 34 51.81	-36 09 47.1	9.0±0.5	9.1±0.6 total	Core	No
NGC 1386	03 34 51.82	-36 09 47.6	1.3±0.1	-	South	-
NGC 2110	05 49 46.38	-07 28 02.0	50.8 ±2.5	81.7±4.1	Core	Decline
NGC 2110	05 49 46.39	-07 28 00.4	32.1±1.6	33.4±1.7	North Jet	No
NGC 2110	05 49 46.37	-07 28 03.5	16.7 ±1.1	15.8±1.1	South Jet	No
Mrk 620	06 45 37.63	+60 54 12.8	7.1±0.4	6.9±0.4	Core (East)	No
Mrk 620	06 45 37.50	+60 54 12.9	2.5±0.2	2.9±0.4	West	No
Mrk 620	-	-	~3.9	-	Ext. NE & SW	-
NGC 3516	11 03 22.81	+72 50 20.5	2.5±0.17	4.1±0.2 total	Core	No
NGC 3516	11 03 22.84	+72 50 20.8	1.4±0.23	-	North	-
NGC 4968	13 04 23.92	-23 24 35.0	6.1±0.4	7.4±0.4 total	Core	No
NGC 4968	13 04 23.88	-23 24 35.2	1.7±0.6	-	West	-
NGC 7465	22 59 32.03	+15 41 44.4	~0.8	1.4±0.1 total	Core	No
NGC 7465	-	-	~0.4	-	NW extension	-

Note. Galaxy name (column [1]), radio component position (column [2]), radio component flux density in 1992 and 1999 (columns [4],[5]), component identification (column [6]), variability between 1992 and 1999 (column [7]).

1999 is probably a result of the more reliable imaging of the extended component in the present data. As shown in Table 3 the nuclear flux density is 9.0 mJy, with an additional 1.3 mJy in the southern extended component.

Ionised gas lies in a string of emission-line knots extending more than 2'' (180 pc) north and south of the nucleus in a direction similar to that of the extended radio emission. However, comparison of the [O III] and radio images (Figure 5) shows no direct association between radio and optical components.

NGC 2110 (type 2) - The previously known (Ulvestad & Wilson 1983; Ulvestad & Wilson 1984; Nagar et al. 1999) symmetrical curved jet-like features extending north and south of the nucleus are clearly visible in Figure 1. The fainter, inner 1'' (150 pc) of the radio jets appear straight and well collimated before changing direction at the brighter hot-spots ~1.5'' from the nucleus. In addition, the lower resolution, naturally weighted image reveals a weaker, more diffuse component extending away from each jet end, most noticeable in the south-west, possibly indicating disruption and de-collimation of the radio jets or an extended radio cocoon flowing along the galactic density gradient. We

do not detect any significant extended nuclear emission perpendicular to the radio jets and conclude that the small extension to the east of the nucleus seen by N99 is probably an imaging artefact due to the limited (u, v) coverage of their snapshot observations.

The flux density of nucleus has declined by 30.9 mJy or ~38% in seven years, while the flux density of the radio jets, has, as expected, remained constant over this period, increasing our confidence in the variability measurement of the nucleus. NGC 2110 is the only Seyfert in this sample with significant *extended* radio emission and a variable nucleus suggesting that the value of ~38% variability is a lower limit; detection of such a variation in flux density, despite contamination by unresolved jet emission, implies very strong radio flux variability in the inner <0.1'' (~15 pc).

The relationship between the ionised gas and radio emission has been investigated by Mulchaey et al. (1994), Ferruit et al. (1998), and Ferruit et al. (2004).

Mrk 620 (NGC 2273) - Seyfert type 2 - The radio emission from Mrk 620 (Figure 2) consists of an east-west double source with weaker, extended emission to the north-east and south-west (see also Figure 6 :left).

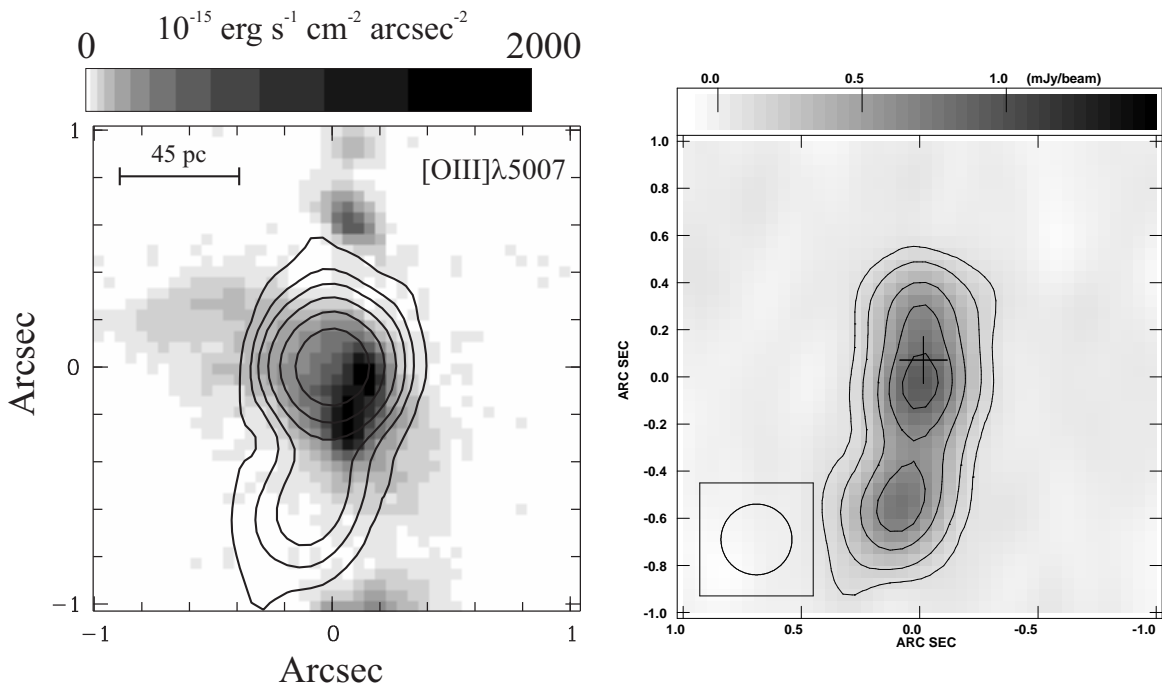


FIG. 5.— Left: 8.4-GHz radio continuum image of NGC 1386 (contours) overlaid on the *HST* [O III] λ 5007 Å image from Ferruit et al. (2000) (grey). The range in [O III] intensity, as indicated by the grey-scale bar above the image, is $0\text{--}2\times 10^{-12}$ ergs s^{-1} cm^{-2} arcsec^{-2} . Contour levels for the 8.4-GHz radio emission are (1, 3, 6, 12, 24, 48) $\times 83$ $\mu\text{Jy beam}^{-1}$; Right: 8.4-GHz residual radio image of NGC 1386 after subtraction of a point source of flux 7.3 mJy; the position of the subtracted point source is marked “+”. Contour levels are (-1, 1, 2, 4, 6, 8) $\times 0.1$ mJy beam^{-1} .

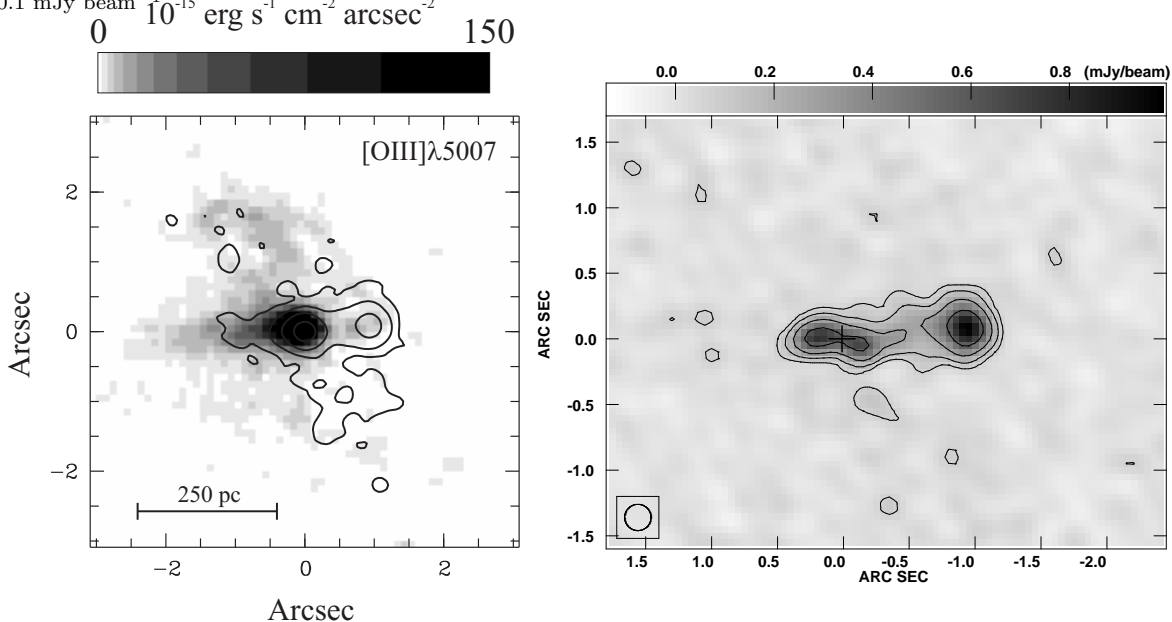


FIG. 6.— Left: 8.4-GHz radio continuum image of Mrk 620 (contours) overlaid on the *HST* [O III] λ 5007 Å image from Ferruit et al. (2000) (grey). The range in [O III] intensity, as indicated by the grey-scale bar above the image, is $0\text{--}1.5\times 10^{-13}$ ergs s^{-1} cm^{-2} arcsec^{-2} . Contour levels for the 8.4-GHz radio emission are (1, 4, 16, 64) $\times 55.2$ $\mu\text{Jy beam}^{-1}$; Right: 8.4-GHz residual radio image of Mrk 620, after subtraction of a point source of flux 7.1 mJy; the position of the subtracted point source is marked with a “+”. Contour levels are (-1, 1, 2, 4, 8) $\times 71.6$ $\mu\text{Jy beam}^{-1}$.

The position of the optical nucleus is close to the eastern component, suggesting it is the nuclear radio component (N99). However, it is also possible that the nucleus lies between the two radio sources. The east component has a slightly flatter spectrum, derived from matched-resolution MERLIN (1.4 GHz) and VLA (8.4 GHz) images ($\alpha_{1.4}^{8.4}(\text{E}) \sim 0.6$, where $S_\nu \propto \nu^{-\alpha}$) than the western component ($\alpha_{1.4}^{8.4}(\text{W}) \sim 0.7$). However, significant ex-

tended flux is also present, making a reliable estimate of spectral index difficult. The eastern component shows a weak extension $0''.4$ to the east and a stronger western extension reaching $\sim 0''.8$ and connecting to the western component of the double (Figure 2). Gaussian fitting to the eastern component shows that it is unresolved perpendicular to the source axis, but is extended along P.A. 81° ; this extended emission is clearly visible in Fig-

TABLE 4
PARAMETERS FOR CONTOUR PLOTS IN FIGURES 1 - 4.

Galaxy	Beam Size (arcsec)	$3 \times \text{rms}$ ($\mu\text{Jy beam}^{-1}$)	Contour levels (in multiples of $3 \times \text{rms}$)
<i>Figure 1</i>			
Mrk 607	0.27×0.27	39.0	(-1, 1, 2, 4, 8, 16)
	0.21×0.21	54.0	(-1, 1, 2, 4, 8, 16)
NGC 1386	0.45×0.45	54.7	(-1, 1, 2, 4, 8, 16, 32, 64, 128)
	0.30×0.30	83.0	(-1, 1, 2, 4, 8, 16, 32, 64)
NGC 2110	0.45×0.45	54.2	(-1, 1, 2, 4, 8, 16, 32, 64, 128, 256)
	0.22×0.22	98.0	(-1, 1, 2, 4, 8, 16, 32, 64, 128, 256)
<i>Figure 2</i>			
Mrk 620	0.30×0.30	55.2	(-1, 1, 2, 4, 8, 16, 32, 64)
	0.20×0.20	71.4	(-1, 1, 2, 4, 8, 16, 32, 64)
MCG-5-23-16	0.42×0.42	37.1	(-1, 1, 2, 4, 8, 16, 32)
	0.30×0.30	60.0	(-1, 1, 2, 4, 8, 16)
NGC 3081	0.44×0.44	50.0	(-1, 1, 2, 4, 8)
	0.32×0.32	75.0	(-1, 1, 2, 4)
<i>Figure 3</i>			
NGC 3516	0.32×0.32	125	(-1, 1, 2, 4, 8, 16)
	0.25×0.25	144	(-1, 1, 2, 4, 8, 16)
NGC 4117	0.31×0.31	43.3	(-1, 1, 2, 4)
	0.23×0.25	55.2	(-1, 1, 2, 4)
NGC 4968	0.39×0.39	63.0	(-1, 1, 2, 4, 8, 16, 32, 64)
	0.30×0.30	75.1	(-1, 1, 2, 4, 8, 16, 32, 64)
<i>Figure 4</i>			
NGC 5273	0.25×0.25	42.1	(-1, 1, 2, 4)
	0.19×0.19	66.0	(-1, 1, 2)
NGC 7465	0.26×0.24	31.8	(-1, 1, 2, 4, 8, 16)
	0.19×0.18	48.2	(-1, 1, 2, 4, 8)
MCG-6-30-15	0.48×0.48	50.0	(-1, 1, 2, 4, 8)
	0.35×0.35	63.0	(-1, 1, 2, 4)

ure 6(right), in which emission from the unresolved point source has been removed. Table 3 lists measured positions and flux densities for the eastern (probably nuclear) and western components; the nuclear flux density shows no variation between 1992 and 1999 (Table 3).

The *HST* [OIII] image (Ferruit et al. 2000) shows high-excitation gas with a one-sided jet-like structure extending along the same east-west direction as the radio emission, along with fainter [OIII] emission extending north-east and southwest of the nucleus. Poor relative astrometry between *HST* optical and radio reference frames makes exact registration of radio and optical structures uncertain; if the eastern radio peak is assumed to be the nucleus and aligned with the [OIII] peak, as was done in Figure 6(left), the [OIII] jet-like feature extends east of the nucleus, where little extended radio emission is detected, and the radio emission extends primarily west of the nucleus, where little high-excitation optical emission is detected. Alternatively, the western radio component could coincide with the peak in the [OIII] emission (resulting in the eastern radio component being $\sim 0''.6$ east of the [OIII] peak), suggesting that the [OIII] peak could be excited by the impact of the radio jet on NLR gas.

In addition to the east-west double radio emission, we estimate a further ~ 3.9 mJy of flux to be present in the diffuse extended radio emission seen to the north-east and southwest of the double source (Figure 2). This diffuse gas might represent back flow from radio jets inferred to power the east-west double, or a less energetic, poorly collimated outflow wind from the nucleus, similar to structures seen in NGC 4051 (Kukula et al. 1995; Christopoulou et al. 1997).

MCG -5-23-16 (ESO 434-G40) - Seyfert type 2 - This source, which was not observed by N99, is well detected

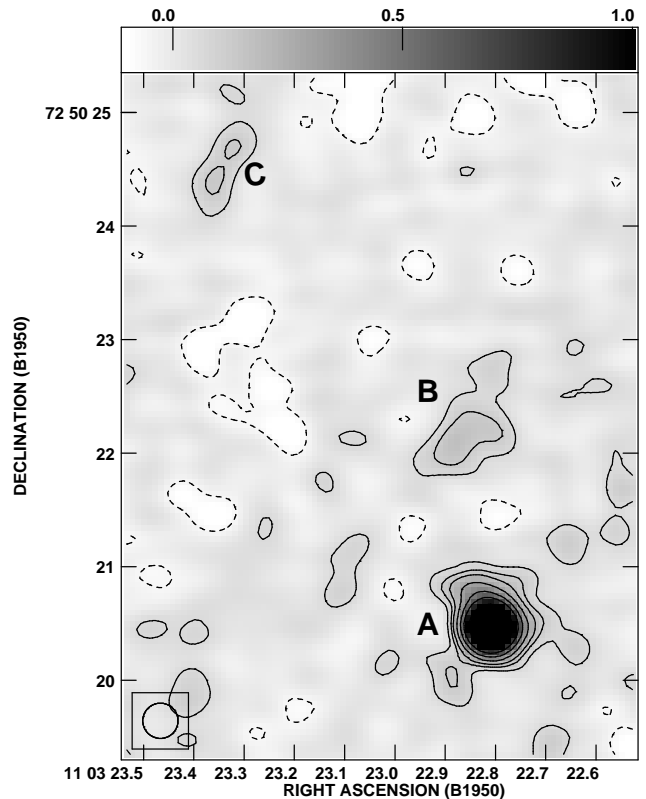


FIG. 7.— Extended emission in NGC 3516; components A, B, C, as identified by Miyaji et al (1992) at $\lambda 6$ cm and $\lambda 20$ cm, are labelled. Data were weighted with a 600k λ taper in order to emphasise these weak components; contour levels are plotted as multiples of $1.5\text{-}\sigma$ at (-1, 1, 2, 3, 5, 8, 12, 20, 28, 36)*60 $\mu\text{Jy beam}^{-1}$.

in our data at a level of $70\text{-}\sigma$ (peak flux). Weak diffuse emission is detected in the naturally weighted image (Figure 2, left), in which the integrated flux density is 20% higher than the peak. A Gaussian fit to the naturally-weighted image suggests the source, with a size of 320 mas (58 pc), is marginally resolved in PA $\sim 169^\circ$. [O III] emission is elongated on either side of the nucleus in P.A. 40° (Ferruit et al. 2000) and does not appear to be related to the marginally extended radio emission.

NGC 3081 - Seyfert type 2 - The radio flux density in this source has declined by 47% between 1992 and 1999. The integrated flux density measured in the naturally-weighted image is slightly higher than the peak, suggesting the presence of extended emission, and the source appears to be marginally resolved with a deconvolved size of ~ 260 mas (44 pc) in P.A. -12° ; this P.A. is similar to the approximate north-south extension of [OIII] emission, but residual imaging artefacts in the radio image make these structure estimates tentative.

NGC 3516 - Seyfert type 1.2 - The measured total flux in 1999 compares well with that in 1992 (Table 2), but we are now able to decompose the emission into two components; 2.5 mJy of emission is associated with the unresolved nucleus and 1.4 mJy from a small component $\sim 0''.3$ north-east of the nucleus. We cannot, therefore, rule out variability of the nucleus between 1992 and 1999,

but it is more likely that the total flux measured in the 1992 data includes both components and the nucleus has remained constant over this period. As described in Section 2, NGC 3516 was observed in spectral line mode to reduce bandwidth smearing effects and allow the removal of contaminating emission from a strong confusing source 4.3 away, which reduced the imaging capabilities of N99; this technique worked well, although low level contamination is still present resulting in a measured rms in the final images that is slightly higher than the theoretical expectation. To test the robustness of our imaging, a heavily tapered image was created; as can be seen in Figure 7, our 8.4 GHz image compares well with previous images made at $\lambda 20$ cm and $\lambda 6$ cm by Miyaji et al. (1992) - components A, B and C, following the nomenclature of Miyaji et al. (1992) are clearly visible. The close correspondence between optical and radio structures in the inner $\sim 4''$ in NGC 3516 is discussed in detail by Ferruit et al. (1998).

NGC 4117 - Seyfert type 2 - NGC 4117 was not detected at 8.4 GHz in 1992 by N99, but is clearly detected in our 1999 data (Figure 3). Following careful reprocessing of the 1992 data, we confirm that this source is undetected and that atmospheric decorrelation is not responsible for its non-detection. We detect no emission above a $3\text{-}\sigma$ level of $90\mu\text{Jy}$ in the 1992 data (providing a very conservative upper limit < 0.1 mJy); in contrast, we detect a peak flux density at a $\sim 15\text{-}\sigma$ level of ~ 0.25 mJy (Figure 3) in the 1999 data. The source is unresolved and still easily detected in the noisier uniform image (Figure 3).

The unresolved radio emission is consistent with the compact [O III] emission. The more extended, lower excitation [N II+H α] emission (Ferruit et al. 2000) seems to correspond to patches of non-nuclear radio emission seen in the 1.4-GHz image of N99 and is likely to be related to star-formation rather than AGN processes.

NGC 4968 - Seyfert type 2 - No variability in the nuclear flux density of NGC 4968 was detected between 1992 and 1999; the slightly higher total flux density (7.8 ± 0.7 mJy) listed for the source in 1999 in Table 2 includes the nuclear flux density of 6.1 mJy (consistent with the peak nuclear flux in the 1992 data of 6.2 ± 0.3 mJy) and an additional 1.7 mJy of emission from a component extending up to $\sim 1''$ west of the nucleus (Figure 3). This extended component was tentatively identified by N99 and is confirmed here; it does not appear to correspond to any ionised gas feature, although dust obscuration west of the nucleus might explain the lack of detectable optical emission in this region (see Figure 14 in Ferruit et al. 2000).

MCG -6-30-15 (ESO 383-G35) - Seyfert type 1.2 - The flux density of this source, measured to be 0.64 mJy in our naturally-weighted image (Figure 4), appears to have declined by $\sim 36\%$ since 1992. However, the integrated flux density measured in the naturally-weighted image is 1.8 times greater than the peak, suggesting the presence of extended emission; the source appears to be marginally resolved with a deconvolved size of ~ 610 mas in P.A. 0° . The source is also clearly detected in the uniformly-weighted image (Figure 4) with a peak flux density of 0.33 mJy (i.e. 14σ). A low resolution tapered image was made, using a 400-k λ taper, to search for additional extended emission; the integrated flux density in

the tapered image (not shown) is 0.81 ± 0.07 mJy, close to but still lower than the value measured in 1992. The low declination of this source results in a highly elongated beam, particularly for snap-shot observations, and may account for N99's conclusion that this source is unresolved.

Extended nuclear [O III] emission in MCG -6-30-15 has been attributed to emission from an inclined nuclear disk (Ferruit et al. 2000, their Figure 17) and therefore is not expected to have any associated non-thermal radio emission. Although the structure of the extended radio emission is not well determined, our data suggest a possible elongation approximately perpendicular to the [O III] disk, as would be expected from a jet-like or disk-driven wind component. Future sensitive, high-angular resolution observations of this source are required to separate extended and compact radio components and to determine the nature of the nuclear flux density variability.

NGC 5273 - Seyfert type 1.5 - The nuclear flux density of this source has declined by $\sim 40\%$ between 1992 and 1999 (Table 2). Gaussian fits by N99 suggested the presence of some marginally extended emission in P.A. $\sim 170^\circ$ and Ulvestad & Wilson suggested P.A. $\sim 5^\circ$. We confirm the presence of extended emission. A Gaussian fit to our naturally-weighted image (Figure 4) yields an integrated flux density that is 1.6 times greater than the peak, with a deconvolved size of 240×133 mas extended in P.A. $\sim 177^\circ$, consistent with the north-south extension seen in ionised gas. Emission in the uniform image is marginally resolved in P.A. $\sim 167^\circ$ (Figure 4).

NGC 7465 (Mrk 313) - Seyfert type 2 - Our measured total flux of 1.2 mJy is consistent with that measured in 1992 (Table 2), indicating no variability between 1992 and 1999. As can be seen in the naturally-weighted image (Figure 4), and also tapered images (not shown), this weak source consists of an unresolved nucleus and extended emission to the north-east and possibly south-west. Gaussian fitting to the naturally weighted image suggests a nuclear source size of 300×200 mas (42×28 pc) in P.A. 33° with a flux density of ~ 0.8 mJy, with an additional 0.4 mJy in extended emission. The higher resolution uniform image shows a curved structure which suggests extension along this same P.A., although Gaussian fitting suggests a P.A. closer to 20° . The exact decomposition of extended and compact emission fluxes is uncertain (Table 3) making it difficult to completely rule out nuclear variability; future observations of this source may provide confirmation of its nuclear behaviour.

Regions of high excitation optical line emission in the inner $2''$ (Ferruit et al. 2000, Figure 25) are elongated in the southeast-northwest directions, roughly perpendicular to the extended radio emission.

4. DISCUSSION

The primary power source for nuclear emission from radio-quiet AGN has long been a matter of debate, but evidence is mounting in favor of accretion by a central supermassive black hole over compact nuclear starbursts. In particular, the presence of well-collimated radio jets in some sources provides strong support for the central black hole plus accretion disk model (Ulvestad et al. 1999; Kukula et al. 1999; Mundell et al. 2003), with the accretion flow and jet forming a natural symbiosis (Falcke & Biermann 1995;

Falcke & Biermann 1999); detection of radio nuclei with flat radio spectra and high brightness temperatures ($T_B > 10^8$ K) in Seyferts (Mundell et al. 2000), LLAGN (Nagar et al. 2002) and radio-quiet quasars (RQQs; Blundell & Beasley 1998) further supports this paradigm.

Nuclear flux variability can provide important additional constraints on central engine physics, but few surveys of radio variability in radio quiet AGN, particularly Seyferts, exist. Falcke et al. (2001) conducted a study of 8.4-GHz radio emission from 30 radio-quiet and radio-intermediate quasars selected from the PG quasar sample and found that $\sim 80\%$ of the sources show at least marginal evidence for variability over a two year period, with some sources showing significant month-to-month variability and a possible trend for greater variability to be seen in nuclei with more inverted spectra. These results support an AGN origin for the radio emission and suggest the presence of relativistic parsec-scale radio jets in the RQQs with the strongest intra-year variability.

4.1. Radio Variability, Seyfert Type and Nuclear Structure

As described in Section 3, five out of eleven Seyferts in our sample show nuclear flux variation over a seven year period. We find no correlation between the detection or degree of variability and Seyfert type: although the sample is small and dominated by Seyfert type 2s, variability is detected in three out of eight type 2 Seyferts and two out of three Seyfert 1.2/1.5s. In radio-loud objects, radio variability is strongest in objects viewed along the line of sight close to the direction of a relativistic jet (blazars, OVV quasars). In the context of the unified scheme, such objects would be of type 1. However, proper motion measurements of Seyfert radio components on the parsec and sub-parsec scale reveal non-relativistic motions (e.g. Ulvestad et al. 1999; Roy et al. 2000; Middelberg et al. 2004; Ulvestad et al. 2005), so amplification by bulk relativistic motion may not occur. Thus the physical nature of nuclear radio variability may be different in radio-loud and radio-quiet AGN. A study of a larger sample of Seyferts, less dominated by type 2s, is required to investigate further whether there is any difference between the radio variability properties of type 1 and type 2 Seyferts.

There is also no correlation between the detection of variability and core luminosity, which lies in the range $8.2 \times 10^{18} < L(\text{core})_{8.4 \text{ GHz}} < 5.9 \times 10^{21} \text{ W Hz}^{-1}$ for this sample, but we do find a correlation between variability and radio compactness. All variable sources, except NGC 2110, are either unresolved or only tentatively marginally resolved, while flux densities of core components in resolved or linear sources are constant at the two epochs. This suggests that all Seyferts might exhibit variation in their nuclear radio flux density at 8.4 GHz, but that variability is more easily recognized in compact sources in which emission from the variable nucleus is not mixed with unresolved, constant flux density radio-jet emission within the central $\lesssim 50$ pc (i.e. the ~ 0.2 typical VLA beam size for $V_{\text{sys}} < 4000 \text{ km s}^{-1}$). The increased detection rate of flat spectrum nuclear radio emission in Seyferts imaged with VLBI resolution (Middelberg et al. 2004) further emphasises the importance of isolating nuclear emission from jet emis-

sion. Linear resolution limitations for studies of more distant AGN such as RQQs are more acute. Barvainis et al. (2005) find, on average, few differences between radio-loud quasars (RLQs) and RQQs other than an unexpectedly-weak dependence of radio variability on nuclear spectral index, with RQQs showing on average steeper spectral indices than RLQ. If RQQs have extended, but unresolved steep spectrum emission similar to that seen in Seyferts, their nuclear variability and nuclear spectral index might also have been underestimated, thus further increasing their similarity to radio-loud AGN.

4.1.1. Nuclear Flare in NGC 2110?

NGC 2110 is unusual as the only Seyfert in this sample with significant extended radio emission *and* a variable nucleus, suggesting that the intrinsic nuclear variability may be higher than the observed $\sim 38\%$. As can be seen in Figure 1, NGC 2110 has striking extended radio structure in the form of curved symmetrical radio jets extending $\sim 4''$ north and south of a compact central flat-spectrum nucleus (see also Ulvestad & Wilson 1983; Ulvestad & Wilson 1984; Nagar et al. 1999). On the smallest scales, Mundell et al. (2000) identified the nucleus at 8.4 GHz as an 8-mJy point source with a maximum size of 0.14×0.07 pc and brightness temperature in excess of 6.0×10^8 K, consistent with synchrotron self absorption and a black-hole driven central engine. They also resolved extended emission ~ 0.7 mas (0.1 pc) north and south of the nucleus consistent with emission from the inner regions of the northern and southern jets, and a discrete component ~ 1.95 mas (~ 0.3 pc) north of the nucleus, possibly the first knot in the northern jet. The nuclear flux variability measured with the VLA clearly indicates a significant change in the structure of the nucleus on scales smaller than the VLA beam size, within the central ~ 0.1 (15 pc), between the two epochs, possibly due to fading of an earlier flare in which new components or shocks in the jet may have appeared. Multi-epoch, multi-frequency VLBA imaging of the nuclear regions would establish the cause of the variability and determine whether new components are emerging in the jet flow during periods of increased nuclear flux density.

4.2. Nuclear Flares and Radio Jets

We are unable to quantify the minimum timescale of variation due to the relatively long time between our two epochs of 8.4-GHz observations. However, the serendipitous discovery of variation in $\sim 50\%$ of our sample, which was not selected on any given radio property or known variability, suggests that radio variability in Seyfert nuclei may be a common phenomenon and that the measured amplitudes of variation are likely to be lower limits to peak-to-peak variations within this period.

In radio-loud objects, the bulk relativistic flow in powerful radio jets is thought to play a key role in Doppler boosting the amplitude of nuclear flux variation and compression of variation timescales, thus enhancing the observed flux variability in blazars whose jets are viewed close to the ejection axis. Long-term radio monitoring of radio-loud AGN (e.g. Hughes et al. 1992; Valtaoja et al. 1992) has demonstrated the existence of stochastic, non-random flare events at centimeter and millimeter wavelengths, with mean timescales of 1.95 and

2.35 years for BL Lac objects and QSOs respectively (e.g. Hughes et al. 1992). In standard jet-shock models, the increases in total flux density are attributed to the passage of shocks on parsec-scales in collimated, relativistic flows and, in some cases, outbursts in monitoring data are seen to correspond to propagation of individual components in VLBI maps.

In contrast, the debate continues over the nature of the ejected radio plasma in Seyferts; the presence of bulk relativistic motion has not yet been demonstrated in Seyfert jets, with existing proper motion studies measuring apparent radio component speeds $V_{app} \lesssim 0.25 c$ (Ulvestad et al. 1999; Roy et al. 2000; Roy et al. 2001). The observations of one-sided parsec-scale jets can be explained by free-free absorption by ionized gas in a disk or torus along the line of sight to the counterjet, rather than Doppler de-boosting/dimming (Ulvestad et al. 1999). Nevertheless, despite the lack of systematic long-term monitoring of Seyferts, radio flares have been detected in a small number of Seyfert nuclei.

A 10-year monitoring study of the 8.4-GHz nuclear radio emission in the double radio-lobed Seyfert 1 galaxy NGC 5548 (Wrobel 2000) revealed photometric variations of 33% and 52% between VLA observations separated by 41 days and 4.1 years respectively. In addition, during the 41-day flare the nucleus exhibited an inverted spectrum with spectral index $\alpha \sim -0.3$ ($S_\nu \propto \nu^{-\alpha}$) compared with the steeper value $\alpha \sim 0.2$ prior to the flare. The flare characteristics support a black-hole driven central engine for the origin of the radio emission with the spectral inversion possibly arising from brightening in the optically-thick base of the parsec-scale radio jet; efforts continue to detect a secondary ejected component.

More dramatic radio flares and inverted radio spectra have been detected in Mrk 348 and III Zw 2 (e.g. Brunthaler et al. 2005). The variable compact radio nucleus of the Seyfert 2 galaxy Mrk 348 (e.g. Sramek & Tovmassian 1974; Neff & de Bruyn 1983) showed increases in continuum flux density by factors of 1.7 at 5 GHz and 5.5 at 15 GHz during the 1982.3–1983.3 and 1997.10–1998.75 periods respectively (Neff & de Bruyn 1983; Ulvestad et al. 1999); bright H₂O megamaser flares were also detected in 2000 and 2001 (Falcke et al. 2000; Peck et al. 2001). In III Zw 2, the high radio frequency light curves (22 GHz and 43 GHz) measured over a ~ 20 year period show a number of radio flares; of particular note was the flare in 1998 that showed a ~ 30 -fold flux increase within two years and a highly-inverted radio spectrum peaking at millimeter wavelengths (Aller et al. 1985; Falcke et al. 1998); similar flares are evident at earlier epochs over the last ~ 25 years at lower frequencies (Brunthaler et al. 2005). A sudden change in spectral shape in 1999, with the frequency of the flux peak dropping quickly from 43 GHz to 15 GHz within a few months, indicated a structural change in the nucleus; this was confirmed by high resolution imaging of the nucleus that revealed a newly ejected radio component expanding at an apparent superluminal speed $V_{app} \gtrsim 1.25 c$ (Brunthaler et al. 2000), in stark contrast to the upper limit of 0.04 c measured during quiescence. Brunthaler et al. (2003) suggest that III Zw 2 flares approximately every five years; this timescale is consistent with the variability detected for Seyferts in our sample, given that two-epoch obser-

vations are more likely to detect fading sources if the decay timescale is longer than the brightening timescale, but shorter timescale variations, such as those seen in quasars (Barvainis et al. 2005) cannot be ruled out.

4.2.1. *Origin of Radio Flares: Jet-Cloud Interactions?*

Due to the small number of detailed studies of Seyfert nuclei in radio outburst, particularly the lack of parsec to sub-parsec scale imaging, the origin of such flares is not yet known. It has been suggested that shocks produced by interaction of a relativistic jet with dense circumnuclear gas clouds within the central parsec might be responsible for the flares, with in situ particle re-acceleration in the shock producing brightening radio emission and inverted spectra (Falcke et al. 1999). For III Zw 2, the initial flux density increase and inverted spectrum with a low jet speed have been likened to similar properties of Gigahertz-Peaked-Spectrum (GPS) sources, in which ultra-compact hot spots are powered by a relativistic jet interacting with circumnuclear clouds (Brunthaler et al. 2003). The subsequent observed phase of superluminal expansion might then correspond to the jet breaking free and propagating relativistically into a lower-density medium (Brunthaler et al. 2000).

Water vapour megamaser flares may also be consistent with a jet-cloud interaction scenario in Seyfert nuclei. Falcke et al. (2000) argued that the megamaser flare in Mrk 348 was driven by a corresponding increase in the continuum emission and suggested the line responded to the continuum flare within ~ 2 -years. The upper limit to the line response time implies the masers lie within $\lesssim 0.6$ pc of the nucleus, a size confirmed by direct, high-resolution imaging (Peck et al. 2001). This imaging showed the maser emission lies ~ 0.4 pc north of the nucleus towards the northern jet, rather than in a nuclear disk perpendicular to the jet. Large H₂O linewidths on these small spatial scales are consistent with the H₂O emission arising from a shocked interface between energetic jet material and the intervening molecular gas cloud, a scenario further supported by spectral evolution mimicking that seen in III Zw 2, with a shift in spectral peak to lower energies at later times (Peck et al. 2001). NGC 1052 shows similar jet-aligned masers (Claussen et al. 1998) consistent with an impact between the jet and a molecular cloud.

More circumstantially, the bright shock-like features in the radio continuum structure of the jet in NGC 4151 have been attributed to the interaction of a well-collimated jet with circumnuclear clouds of diameter < 1.4 pc (Mundell et al. 2003); stringent upper limits on radio component speeds are consistent with the jet being slowed to sub-relativistic speed on scales significantly smaller than ~ 3 pc (Ulvestad et al. 2005).

4.3. *Intermittent Nuclear Quiescence and Outburst*

Key outstanding questions remain on the speeds of Seyfert radio jets, the nature of radio variability in Seyfert nuclei and the relationship between the two. Radio variability and spectral evolution studies offer valuable tools to probe the nuclear radio emission in large numbers of Seyfert nuclei, before following up objects in outburst with high resolution, VLBI imaging. The

ejection speeds of Seyfert jets may turn out to be intrinsically non-relativistic. However, the low radio component speeds measured in the early phase of the flare in III Zw 2 might have important implications for interpretation of sub-relativistic speeds measured in other Seyferts, such as Mrk 348 and Mrk 231 (Ulvestad et al. 1999), in which the low speeds may indicate observations taken during nuclear quiescence or early outburst stages when the jet is impacting a cloud but has not yet drilled through. The small detection rate ($\sim 7\%$) of H_2O megamaser emission in nearby AGN (e.g. Braatz et al. 1996) and maser variability (Braatz et al. 2004) may, in part, result from variability in the 22-GHz continuum, which is presumed to provide the seed photons for maser amplification, and thus further supporting the paradigm of intermittent periods of quiescence and nuclear outburst across the Seyfert population.

Systematic, multifrequency radio monitoring of a larger sample of Seyfert nuclei over timescales of months to years is required to determine the characteristic timescales and amplitudes of variation and changes in spectral index, as well as any correlations with Seyfert type and radio structure. Rapid follow up of flaring nuclei at other wavelengths, in combination with radio imaging on parsec and sub-parsec scales, would provide valuable insight into structural changes, the possible presence of relativistic flows and their relationship with accretion disk changes during the outburst. Such observations will become increasingly routine with new facilities such as the EVLA, eMERLIN and LOFAR.

5. CONCLUSIONS

We have used the VLA at 8.4 GHz to study the radio continuum emission from a sample of 12 optically-selected, early-type Seyfert galaxies. We find the following:

- All 12 Seyferts are detected with the VLA; five nuclei show a variation in their nuclear flux density since 1992, while six have remained constant (one was not observed in 1992). No correlation is found between Seyfert type and the detection of radio variability. Instead, the compactness of the radio emission seems to be a good indicator of variability. All variable nuclei, apart from NGC 2110, are compact and at best marginally resolved, while nuclei with associated extended radio emission have remained constant.
- NGC 2110 is the only Seyfert in this sample with significant extended radio emission from well-defined radio jets *and* a variable nucleus, suggesting that the intrinsic nuclear variability is higher than the observed $\sim 38\%$. The observed nuclear flux variability indicates significant changes are likely to have occurred in the structure of the nucleus on scales smaller than the VLA beam size (i.e. within the central $\sim 0''.1$ [15 pc]), between the two

epochs, possibly due to the appearance and fading of new components or shocks in the jet. This interpretation is consistent with sub-parsec scale structures identified previously by Mundell et al. (2000) that consist of a high brightness temperature ($> 6.0 \times 10^8$ K), synchrotron self-absorbed point source, extended jet emission 0.1 pc north and south of the nucleus, and a discrete component ~ 0.3 pc north of the nucleus, possibly the first knot in the northern jet.

- The serendipitous discovery of variability in $\sim 50\%$ of our sample, which was not selected on any given radio property or known variability, suggests that radio variability in Seyfert nuclei is a common phenomenon and that the measured amplitudes of variation are likely to be lower limits to peak-to-peak variations within this period.
- We conclude that all Seyferts might exhibit variations in their nuclear radio flux density at 8.4 GHz, but that variability is more easily recognized in compact sources in which emission from the variable nucleus is not mixed with unresolved, constant flux density radio-jet emission within the $\sim 0''.2$ VLA beam size (i.e. the central $\lesssim 50$ pc for $V_{\text{sys}} < 4000$ km s $^{-1}$).
- We speculate that if flares in radio light curves correspond to ejection of new relativistic components or emergence of shocks in the underlying flow, sensitive systematic monitoring of a larger sample, combined with subarcsecond resolution imaging, may confirm that Seyferts - as black-hole driven AGN - have the capacity to accelerate relativistic jets during radio flares despite having radio jets that are intrinsically non-relativistic during quiescence.

This paper is dedicated to A.S. Wilson, a valued colleague, mentor and friend. CGM acknowledges financial support from the Royal Society and Research Councils U.K.; NN acknowledges support from BASAL PFB-06/2007, ALMA 31060013 and Fondecyt 1080324. We thank the anonymous referee for constructive comments that improved the paper. This research was partially supported by NSF grant AST 9527289 to the University of Maryland. The National Radio Astronomy Observatory is a facility of the National Science Foundation operated under cooperative agreement by Associated Universities, Inc. This research has made use of the NASA Astrophysics Data System Abstract Service (ADS), and the NASA/IPAC Extragalactic Database (NED), which is operated by the Jet Propulsion Laboratory, California Institute of Technology, under contract with the National Aeronautics and Space Administration.

REFERENCES

- Aller, H.D., Aller, M.F., Latimer, G.E. & Hodge, P.E. 1985 ApJS, 59, 513
 Barvainis, R., Lehár, J., Birkenshaw, M., Falcke, H. & Blundell, K.M. 2005, ApJ 618, 108
 Blundell, K.M. & Beasley A.J. 1998 MNRAS, 299, 165
 Braatz, J.A., Wilson, A.S. & Henkel, C. 1996 ApJS, 106, 51
 Braatz, J.A., Henkel, C., Greenhill, L.J., Moran, J.M. & Wilson, A.S. 2004, ApJ, 617, L29
 Brunthaler, A. et al. 2000 A&A, 357, L45

- Brunthaler, A., Falcke, H., Bower, G.C., Aller, M.F., Aller, H.D., Teräsranta, H., Krichbaum, T.P. 2003, *PASA*, 20, 126
- Brunthaler, A., Falcke, H., Bower, G.C., Aller, M.F., Aller, H.D. & Teräsranta, H. 2005 *A&A*, 435, 497
- Christopoulou, P.E., Holloway, A.J., Steffen, W., Mundell, C.G., Thean, A.H.C., Goudis, C.D., Meaburn, J. & Pedlar, A. 1997 *MNRAS*, 284, 385
- Claussen, M.J., Diamond, P.J., Braatz, J.A., Wilson, A.S. & Henkel, C. 1998 *ApJ*, 500, L129
- De Robertis, M.M. & Osterbrock, D.E. 1986 *ApJ*, 301, 98
- Falcke, H. & Biermann, P.L. 1995 *A&A*, 293, 665
- Falcke, H. & Biermann, P.L. 1999 *A&A*, 342, 49
- Falcke, H., Wilson, A.S. & Simpson, C. 1998 *ApJ*, 502, 199
- Falcke, H. et al. 1999 *ApJ*, 514, L17
- Falcke, H., Henkel, C., Peck, A.B., Hagiwara, Y., Prieto, A.M. & Gallimore, J.F. 2000 *A&A*, 358, L17
- Falcke, H., Léhar, J., Barvainis, R., Nagar, N. & Wilson, A.S. 2001, in *ASP Conf. Ser. 224 Probing the Physics of Active Galactic Nuclei*, ed. B.M. Peterson, R.W. Pogge & R.S. Polidan (San Francisco: ASP), 265
- Ferruit, P., Wilson, A.S. & Mulchaey, J.S. 1998, *ApJ*, 509, 646
- Ferruit, P., Wilson, A.S. & Mulchaey, J.S. 2000 *ApJS*, 128, 139
- Ferruit, P., Mundell, C.G., Nagar, N.M., Emsellem, E., Pécontal, E., Wilson, A.S. & Schinnerer, E. 2004 *MNRAS*, 352, 1180
- Giozzi, M., Sambruna, R.M. & Eracleous, M. 2003 *ApJ*, 586, L37
- Greisen, E. W., & Murphy, P. P. 1998, in *The AIPS Cookbook*, chap. 9
- Hughes, P.A., Aller, H.D. & Aller, M.F. 1992 *ApJ*, 396, 469
- Lister, M.L. 2001, *ApJ*, 561, 676
- Kukula, M.J., Pedlar, A., Baum, S.A. & O'Dea, C.P. 1995 *MNRAS*, 276, 1262
- Kukula, M.J., Ghosh, T., Pedlar, A. & Schilizzi, R.T. 1999 *ApJ*, 518, 117
- McHardy, I.M., Gunn, K.F., Uttley, P. & Goad, M.R. 2005, *MNRAS*, 359, 1469
- Middelberg, E. et al. 2004 *A&A*, 417, 925
- Miyaji, T., Wilson, A.S. & Perez-Fournon, I. 1992 *ApJ*, 385, 137
- Mulchaey, J.S. et al. 1994 *ApJ*, 433, 625
- Mulchaey, J.S., Wilson, A.S. & Tsvetanov, Z.I. 1996 *ApJS*, 102, 309
- Mundell, C.G., Wilson, A.S., Ulvestad, J.M. & Roy, A.L. 2000 *ApJ*, 529, 816
- Mundell, C.G., Ferruit, P. & Pedlar, A. 2001, *ApJ*, 560, 168
- Mundell, C.G., Wrobel, J.M., Pedlar, A. & Gallimore, J.F. 2003, *ApJ*, 583, 192
- Nagar, N. et al. 1999 *ApJS*, 120, 209 (N99)
- Nagar, N., Falcke, H., Wilson, A.S. & Ulvestad, J.S. 2002 *A&A*, 392, 53
- Nandra, K., Le, T., George, I.M., Edelson, R.A., Mushotzky, R.F., Peterson, B.M. & Turner, T.J. 2000 *ApJ*, 544, 734;
- Neff, S.G. & de Bruyn, A.G. 1983 *A&A*, 128, 318
- Orr, M.J.L. & Browne, I.W.A. *MNRAS*, 200 1067
- Peck, A.B., Falcke, H., Henkel, C. & Menten, K.M. 2001, in *ASP Conf. Ser. 249, The Central Kiloparsec of Starbursts and AGN*, ed. J. H. Knapen, J. E. Beckman, I. Shlosman, & T. J. Mahoney (San Francisco: ASP), 321
- Peterson, B.M., McHardy, I.M. & Wilkes, B.J. 2000 *NewAR*, 44, 491
- Roy, A. L., Wilson, A. S., Ulvestad, J. S. & Colbert, J. M. 2000, in *Proceedings of the 5th European VLBI Network Symposium*, ed. J.E. Conway, A.G. Polatidis, R.S. Booth & Y.M. Pihlström, 7
- Roy, A.L. et al. 2001, in *IAU Symposium 205, Galaxies and their Constituents at the Highest Angular Resolutions*, ed. R. T. Schilizzi, 70
- Sambruna, R.M., Eracleous, M. & Mushotzky, R.F. 1999 *ApJ*, 526, 60
- Shemmer, O. et al. 2001 *ApJ*, 561, 162
- Smith, H.J. & Hoffleit, D. 1963 *AJ*, 68, 292
- Sramek, R.A. & Tovmassian, H.M. 1974 *ApJ*, 191, L13
- Turner, T.J., George, I.M., Nandra, K. & Turcan, D. 1999 *ApJ*, 524, 667
- Ulrich, M-H, Maraschi, L. & Urry, C.M. 1997 *ARA&A*, 35, 445
- Ulvestad, J.S. & Wilson, A.S. 1983 *ApJ*, 264, L7
- Ulvestad, J.S. & Wilson, A.S. 1984, *ApJ*, 285, 439
- Ulvestad J.S., Wrobel, J.M., Roy, A.L., Wilson, A.S., Falcke, H. & Krichbaum, T.P. 1999 *ApJ*, 517, L81
- Ulvestad, J.S., Wong, D.S., Taylor, G.B., Gallimore, J.F. & Mundell, C.G. 2005 *AJ*, 130, 936
- Valtaoja, E., Teräsranta, H., Urpo, S., Nesterov, N.S., Lainela, M. & Valtonen, M. 1992 *A&A*, 254, 80
- Valtaoja, E., Savolainen, T., Wiik, K. & Lähteenmäki, A. 2002 *PASA*, 19, 117
- van Moorsel, G., Kembell, A., & Greisen, E. 1996, in *ASP Conf. Ser. 101, Astronomical Data Analysis Software and Systems V*, ed. G. H. Jacoby & J. Barnes (San Francisco: ASP), 37
- Wandel, A., Peterson, B.M. & Malkan, M.A. 1999 *ApJ*, 526, 579
- Wheatley, J.M., Welsh, B.Y. & Browne, S.E. 2008, *AJ*, 136, 259
- Wrobel, J.M. 2000 *ApJ*, 531, 716